

HEXA-MoE: EFFICIENT AND HETEROGENEOUS-AWARE MoE ACCELERATION WITH ZERO COMPUTATION REDUNDANCY

Shuqing Luo¹ Jie Peng² Pingzhi Li³ Tianlong Chen³

ABSTRACT

Mixture-of-Experts (MoE) has emerged as a practical approach to scale up parameters for the Transformer model to achieve better generalization while maintaining a sub-linear increase in computation overhead. Current MoE models are mainly built with expert parallelism on distributed devices. However, it usually depends on homogeneous devices to deploy and suffers from heavy communication overhead and computation redundancy. In this paper, we explore developing a Heterogeneous-aware EXpert Allocation framework, **HEXA-MoE**, with significantly enhanced computing efficiency. It contains two components: (1) *Expert-Specific Operators*. We replace the typical general matrix multiplication or grouped matrix multiplication interfaces with our operators, which allows the computing to be performed in an in-place manner with **ZERO** redundancy. (2) *Adaptive Data- and Model-Centric Configurations* for different workload scales. Specifically, we introduce a pipeline-shared cache on each device to tackle the heavy memory consumption in the existing data-centric MoE library. Comprehensive experiments on the Swin-MoE benchmark consistently reveal the effectiveness of our HEXA-MoE framework, *i.e.*, reducing 10% ~ 48% memory consumption and achieving 0.5 ~ 4.3 \times speed up compared to current state-of-the-art MoE libraries. Furthermore, we examine our HEXA-MoE with heterogeneous devices for both data- and model-centric settings. Promising results show that employing optimal parallel configuration with HEXA-MoE on heterogeneous devices can substantially minimize overall latency. Codes are available at [here](#).

1 INTRODUCTION

Transformers have become the *de facto* architecture for a vast range of machine learning tasks including natural language process (Vaswani, 2017; Raffel et al., 2020), computer vision (Liu et al., 2021; He et al., 2022b) and multi-modal learning (Li et al., 2022; Liu et al., 2024). To scale up model parameters for stronger learning capacity and better generalization following the scaling law (Kaplan et al., 2020), Mixture-of-Experts (MoE) (Jiang et al., 2024) has been demonstrated as a practical and computation-efficient approach. For a single MoE layer, the feed-forward network (FFN) is expanded to a group of experts compared to the dense counterpart, activated selectively during computing. This dynamic nature poses peculiar challenges to system design. Current MoE frameworks usually present some unique attributes that differentiate them from dense models:

- ❶ Distributed computing is required for MoE due to its sheer size, and expert parallelism (Lepikhin et al., 2020) is the most commonly used technique, which distributes the experts in one layer on different devices.

- ❷ Since the workload varies dynamically for each expert in each layer, we have to re-organize the local data batches for expert computing via dispatch and combine operations. Specifically, we have to calibrate the workload for each expert to utilize the general matrix multiplication (GeMM) or grouped GeMM interface.
- ❸ Since each token may activate any one or several experts and different experts may be distributed on different devices in expert parallelism, it is necessary to communicate among devices before and after each MoE layer via all-to-all communication.

These peculiar designs lead to inefficiency for both training and inference in MoE computing. On the one hand, dispatch and combine operations result in unnecessary token padding or discarding (Gale et al., 2023), leading to both redundant computation and compromise on model performance. Meanwhile, conventional expert parallelism depends on all-to-all communication, which requires synchronization and occupies a lot of latency (Li et al., 2023). On the other hand, current expert parallelism for MoE models is mainly deployed on homogeneous devices. However, a cluster equipped with the latest homogeneous devices is usually much more expensive than heterogeneous devices due to the iteration of GPU development and the decrease on prices for old-version GPUs. If we want to adapt expert

¹Peking University, China ²University of Science and Technology of China, China ³University of North Carolina, Chapel Hill, USA. Correspondence to: Tianlong Chen <tianlong@cs.unc.edu>.

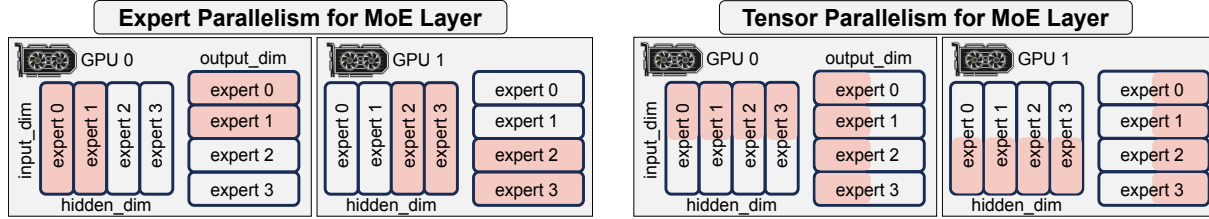


Figure 1: **Tensor Parallelism vs Expert Parallelism for MoE layer.** We take 4 experts on 2 devices as an example and visualize the parameter distribution of 2 MLPs. For expert parallelism, each device can only keep several experts, while for tensor parallelism the parameter allocation is more flexible since the partition of parameters is along the hidden dimension.

parallelism to *heterogeneous* devices, it would be necessary to rearrange the expert distribution to utilize the total computing capacity better. However, the inherent dynamic property of the MoE layer makes it difficult to implement, as the workload of each expert changes dynamically in each step during computing (He et al., 2022a; Li et al., 2023). Meanwhile, since heterogeneous devices are cheaper and easier to access if MoE computing can be re-designed to be heterogeneous-aware, it would benefit wider deployment.

This paper proposes HEXA-MoE, a heterogeneous-aware framework for efficient MoE computing. We first find that if compiling the MoE layer into GeMM like other operators such as Linear, Convolution, *etc.*, the unnecessary components such as token padding or discarding are unavoidable. To tackle it, we investigate the forward and backward propagation for the MoE layer thoroughly, and propose to replace current GeMM or grouped GeMM (Gale et al., 2023) interfaces with expert-specific operators. Specifically, all the computations related to the MoE layer can be summarized as built on 3 operators, *i.e.*, expert-specific matrix multiplication (*ESMM*), expert-specific summation (*ESS*) and expert-specific transposed matrix multiplication (*ESTMM*). The forward propagation only requires *ESMM*, while backward requires all the 3 operators. We implement them in a highly-parallelized manner on GPU, and distribute the MoE layer with tensor parallelism (Narayanan et al., 2021) as an alternative to expert parallelism, shown in Figure 1.

HEXA-MoE also considers different workload scales for MoE computing and is adapted to both data- and model-centric configurations. Specifically, the difference lies in the content of communication. For model-centric, local data batches are synchronized among devices, and model parameters are kept still, while for data-centric, local parameters are gathered to each device, while local data batches are kept still (Liu et al., 2023). When the scale of data is larger than the model parameters, the data-centric setting would perform better. However, previous work preserves all the gathered MoE parameters on each device for backward propagation, leading to huge memory consumption. To achieve better memory efficiency while maintaining high computing speed, we propose to introduce a pipeline-shared cache on each device, which is updated dynamically during

both forward and backward propagation, and the all-gather communication can be overlapped with non-MoE operations such as attention. Essentially, a data-centric setting can be viewed as data parallelism, which is easy to adapt to heterogeneous devices. A model-centric setting is employed when the size of model parameters is larger than the data workload. In this case, all gathered communication is applied to the data batches, and tensor parallelism is applied to each MoE layer. Each device processes all the data batches using the parameter chunk it preserves. This can also be employed in heterogeneous devices via adaptively allocating expert parameters, as illustrated in Figure 1.

Our contributions can be summarized as follows:

- ★ We propose to refactor MoE computing with expert-specific operators, enabling it to be performed in an in-place manner without the requirement of dispatch and combine operations. In this way, **ZERO** computation redundancy would be introduced. We implement these operators in a highly parallelized manner on GPU.
- ★ We develop HEXA-MoE based on the expert-specific operators for both data- and model-centric settings, considering different scales of workload, and propose to employ pipeline-shared cache for data-centric setting to improve memory efficiency. Experiments with Swin-MoE show that HEXA-MoE can reduce 10% ~ 48% memory usage and achieve 0.5 ~ 4.3× speed up compared to state-of-the-art MoE computing libraries.
- ★ Our HEXA-MoE transforms conventional expert parallelism into pure data or tensor parallelism, making it heterogeneous-aware. Experiments show that our HEXA-MoE can be effectively adapted to heterogeneous devices, and employing the optimal parallel configuration can substantially minimize overall latency.

2 RELATED WORKS

Scaling Transformers with MoE. Transformer models can be scaled up via the Mixture-of-Experts (MoE) for better learning capacity and generalization while enjoying a sub-linear increase in computation overhead due to its sparsity. It has been proven in many research fields such as natural language processing (Fedus et al., 2022; Jiang et al., 2024; Du et al., 2022), machine vision (Riquelme et al., 2021; Fan et al., 2022) and multi-modal learning (Bao et al., 2022).

Table 1: Description of symbols.

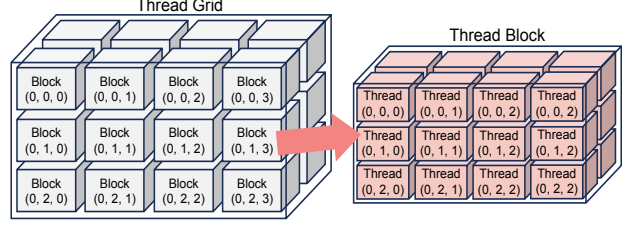
Symbol	Description
E	Number of global experts.
N	Number of the input tokens.
\mathcal{F}	Activation function between the two MLPs.
\mathcal{F}'	Element-wise differential for \mathcal{F} .
\odot	Element-wise product.
D_i, D_o	Input and output size of the FFN.
\mathbf{x}	Data batch with N tokens.
\mathbf{x}^e, N_e	Tokens in \mathbf{x} routed to expert e with number N_e .
$\{\mathcal{R}_i(\mathbf{x})\}_{i=0}^{k-1}$	Routing choice for \mathbf{x} under top- k routing.
$\mathbf{W}_1, \mathbf{W}_2$	Weights for 2 MLPs, shaped as (E, D_1, D_2) .
$\mathbf{b}_1, \mathbf{b}_2$	Biases of the two MLPs, shaped as (E, D) .
BLK	Block size for expert-specific operators.
WARP	Warp size in a thread block.
TIMES	A thread block has $\text{WARP} \times \text{TIMES}$ threads.

Open-Source MoE Computing Libraries. FastMoE (He et al., 2021) pioneered the first PyTorch open-source implementation for distributed MoE. Based on it, FasterMoE (He et al., 2022a) proposes dynamic shadowing and smart scheduling to tackle load imbalance and improve parallelism. Tutel (Hwang et al., 2023) implements switchable parallelism and dynamic pipelining, improving adaptability and scalability. MegaBlocks (Gale et al., 2023) proposes block-sparse operations and corresponding GPU kernels to mitigate dynamic routing issues in MoEs.

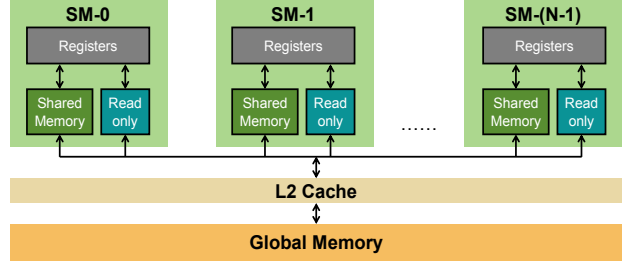
Improving efficiency for MoE computing. MoE computing faces significant challenges in communication and memory. Recent research has explored alleviating them from various perspectives: Lina (Li et al., 2023) proposes to dynamically schedule resources to reduce latency and tackle the all-to-all bottleneck. Janus (Liu et al., 2023) proposes a data-centric paradigm that replaces traditional all-to-all communication with asynchronous expert fetching, enabling overlapped communication and computation for enhanced parallelism. ScheMoE (Shi et al., 2024) proposes a generic scheduling framework for optimal communication and computation scheduling during MoE training. MPMoE (Zhang et al., 2024) accelerates MoE training through adaptive and memory-efficient pipeline parallelism. SmartMoE (Zhai et al., 2023) proposes an efficient searching algorithm to identify optimization opportunities within an expanded hybrid parallelism space, tailored for data-sensitive MoE models. PipeMoE (Shi et al., 2023) adaptively pipelines communications and computations in MoE to mask communication latency. It also provides an optimal strategy to determine pipeline degree to minimize overall iteration time.

3 PRELIMINARY

Introduction to CUDA Programming: A GPU program can be viewed as a thread grid in Figure 2(a), which is 3-



(a) Thread hierarchy for CUDA programming.



(b) Memory hierarchy for a GPU.

Figure 2: Thread hierarchy for CUDA programming and memory hierarchy for a typical NVIDIA GPU.

dimensional and contains massive thread blocks. A thread block is also 3-dimensional and contains up to 1024 threads. Computation is mapped to these threads and implemented in parallel. Physically a GPU is composed of massive streaming multiprocessors (SM), where we show the memory hierarchy in Figure 2(b). Each SM loads data from global memory to its registers for parallel computing, and caching with shared memory can be faster. An SM contains many processing units including CUDA core and Tensor core. The former is used for general parallel computing, while the latter is specialized for matrix multiplication with mixed precision, which is first introduced in NVIDIA Volta architecture (Choquette et al., 2018). During execution, an SM is given one or more thread blocks, which are partitioned into warps and each warp gets scheduled by a warp scheduler.

Mathematical Symbols: We provide the description of mathematical symbols used in this paper in Table 1, including variables in MoE computing and constant values in CUDA programming. To utilize Tensor core for faster matrix processing, we have to call the `nvcuda::wmma` (warped matrix multiplication and add) interface to compute a fixed-sized matrix multiplication such as $16 \times 16 \times 16$ in a single warp, therefore the number of threads in a block has to be divisible by the constant value `WARP`. In the CUDA implementation of our method, a thread block loads `BLK` tokens each time from global memory to shared memory to conduct the parallelized computation.

4 METHOD

We start our exploration by first formulating the forward and backward propagation of a single MoE layer with and without GeMM, which induces the same calculation results

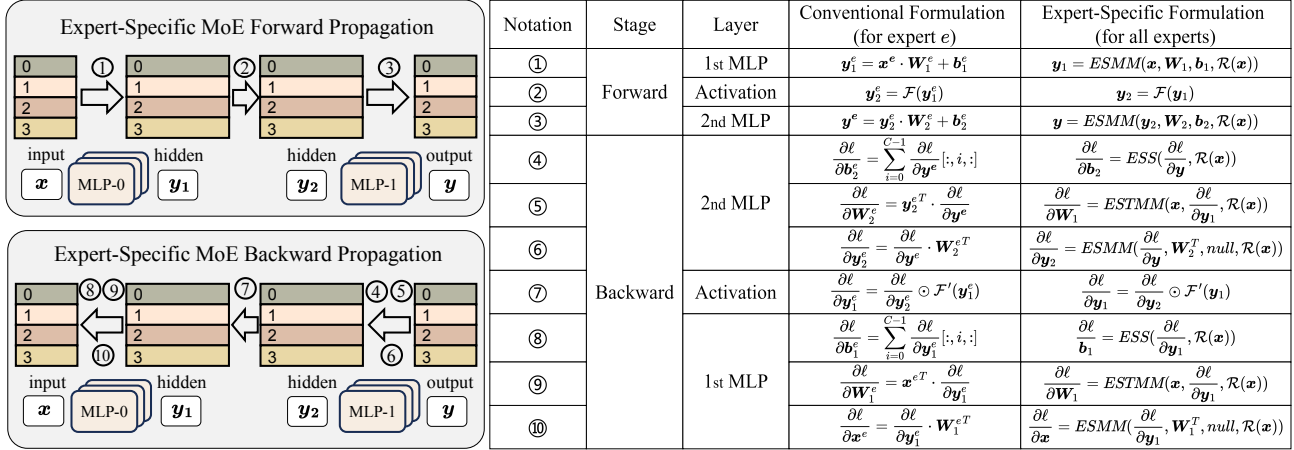


Figure 3: **Comparison between conventional and expert-specific formulation for MoE computing.** We take top-1 routing for illustration and present the corresponding relation of each formula in the MoE forward and backward propagation.

in different ways (Sec. 4.1). Specifically, GeMM-based MoE computing depends on inefficient dispatch & combine operations, while our *expert-specific* operators serve as an alternative, performing in-place and inducing **ZERO** computation redundancy. After that, we expound the details for our optimized CUDA implementation (Sec. 4.2). We also introduce a novel expert-specific fused operator in this part, specialized for parallel MoE backward propagation. These empower our HEXA-MoE with high computation efficiency. Next, we consider different workload scales, and adapt HEXA-MoE efficiently to both *data*- and *model*-centric settings (Sec. 4.3). Finally, we adapt HEXA-MoE to heterogeneous devices, and provide an expert allocation approach to minimize the average latency so as to utilize better heterogeneous computing capacities (Sec. 4.4).

4.1 MoE Computing Formulation

GeMM-based MoE Computing. Current MoE libraries are mainly built on expert parallelism (Fedus et al., 2022) and dispatch & combine operations (Hwang et al., 2023). Specifically, “expert parallelism” means distributing the experts to different devices, “dispatch” means assigning the experts with different tokens based on the routing choice, and “combine” means restoring the original data batch from dispatched tokens. In conventional settings, all-to-all communication is required to further assign the dispatched tokens to the corresponding device, where the corresponding expert is kept. To employ GeMM on each device, we need to calibrate the workload of each expert via token padding or discarding and build a new data batch. Taking top-1 routing as an example, we formulate the forward and backward propagation in Figure 3, denoting ℓ as loss value and x^e as tokens dispatched to expert e (with N_e tokens). In backward propagation, the gradients of the output have been provided by the auto-differentiation program.

Based on dispatch and combine operations, all variables

can be derived via basic matrix operations such as summation and multiplication. Although we can utilize the high-performance GeMM interface, these operations are inefficient, since the workload of each expert varies dynamically in each step, and token padding or discarding has to be employed to construct new data batches for local experts. It can be overcome by our expert-specific design.

MoE Computing via Expert-Specific Operators. Based on the above formulations, we propose to re-implement in an in-place manner to address the inefficient teaser of dispatch & combine operations. Specifically, we find that the forward and backward propagation of a single MoE layer can be reformulated as built upon 3 specialized operators from an expert-specific perspective, namely *expert-specific* operators. We take top-1 routing for illustration, while formulations for top- k routing are provided in Appendix A.

- ① Expert-specific matrix multiplication (*ESMM*): given input batch x with N tokens, routing choice $\mathcal{R}(x)$, weight W and bias b , we formulate it as $y = ESMM(x, W, b, \mathcal{R}(x))$, where y_i is derived from x_{i_i} , as well as the corresponding $W_{\mathcal{R}(x_i)}$ and $b_{\mathcal{R}(x_i)}$. *ESMM* is applied to get the hidden and output tokens in forward, and the gradients of hidden and input tokens in backward propagation, as shown in Figure 4(b).
- ② Expert-specific summation (*ESS*): given input batch x with N tokens and routing choice $\mathcal{R}(x)$, it is formulated as $y = ESS(x, \mathcal{R}(x))$, where tokens routed to expert e are accumulated and recorded in $y[e]$. *ESS* is applied to get the gradients of bias in backward propagation, as illustrated in Figure 4(c).
- ③ Expert-specific transposed matrix multiplication (*ESTMM*): the inputs include two batches x_1 and x_2 (both with N tokens), and the routing choice $\mathcal{R}(x)$. Both x_1 and x_2 are the *ESMM* result of x , thus sharing the same routing choice. It is formulated as $y = ESTMM(x_1, x_2, \mathcal{R}(x))$. For the i -th

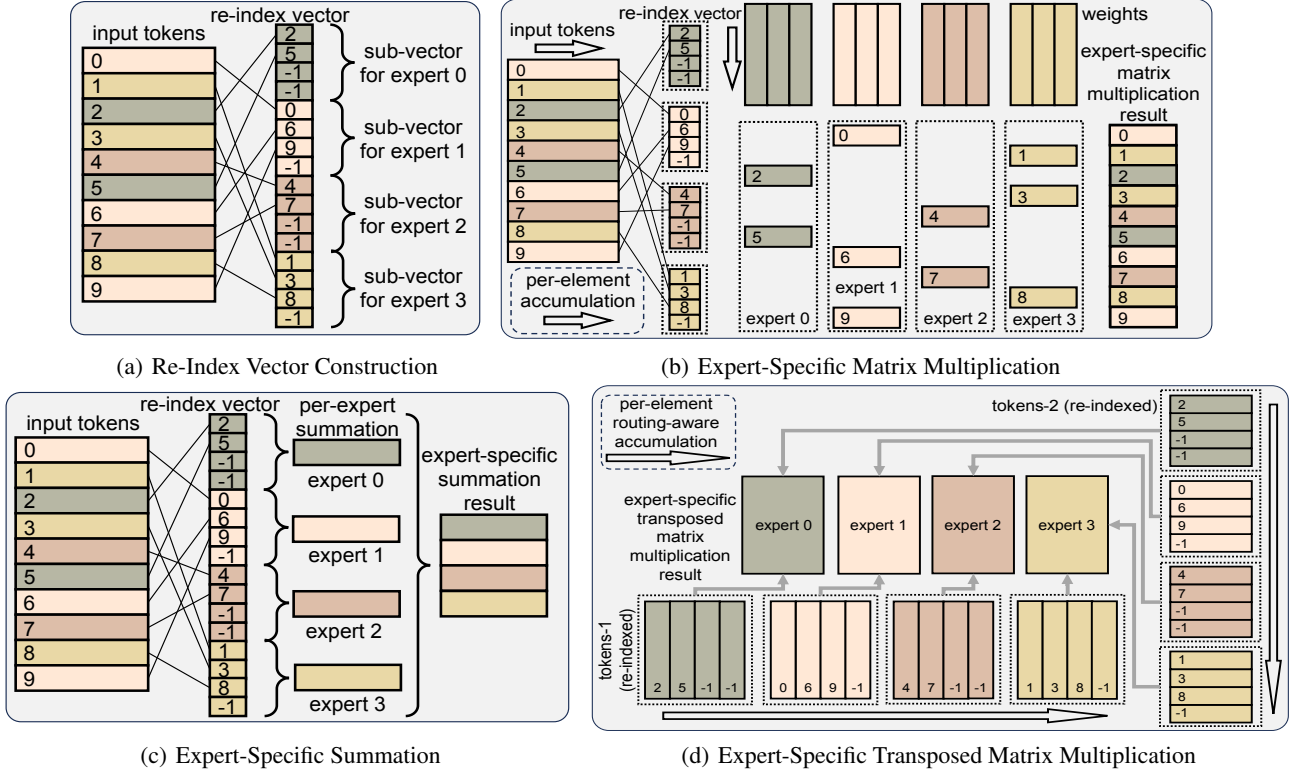


Figure 4: **Illustration of the proposed operators.** Take 10 tokens, 4 global experts, and block size 4 as an example. For *ESTMM*, the 2 input batches are in a re-indexed format, while for others both the raw batch and re-index vector are provided.

channel of x_1 and j -th channel of x_2 , we first prepare a zero vector c with E elements, and accumulate $x_1[m, i] \cdot x_2[m, j]$ to $c[\mathcal{R}(x_m)]$ for all $0 \leq m < N$. After that we assign $c[k]$ to $y[k, i, j]$ for all $0 \leq k < E$. *ESTMM* is applied to get the gradients of weights in backward propagation, as illustrated in Figure 4(d).

Based on these *expert-specific* operators, we can now implement MoE computing in a novel in-place manner, as formulated in Figure 3. We compare each stage between our method and conventional formulation, and the output of each token is ensured to be consistent for both cases. In forward propagation, *ESMM* performs as an alternative to common matrix multiplication, while in backward propagation, the gradient of y is also provided by the auto-differentiation program. *ESS* performs as an alternative to tensor summation, while *ESMM* and *ESTMM* are designed as 2 specialized cases for matrix multiplication from the expert-specific perspective. With the help of our expert-specific design, we can now directly compute the output for all MoE computing tasks rather than dispatching the tokens to each expert before MoE computing, introducing zero redundancy.

4.2 Optimized CUDA Implementations

Re-Index based Expert-Specific Operators. Although expert-specific operators enable MoE computing to be performed in an in-place manner, we should not implement them directly, since simply computing for each token in par-

allel cannot fully utilize the locality of GPU, which restricts the performance. Considering that we cannot guarantee the adjacent tokens to be routed to the same expert, we have to introduce other tensors as auxiliaries. In HEXA-MoE, we additionally adopt a re-index vector, as illustrated in Figure 4(a). Specifically, we re-organize the token indices based on the routing choice, *i.e.*, gathering indices for tokens that routed to the same expert into a sub-vector, and padding it with -1 to make it divisible by a constant value BLK. The algorithm details are provided in Appendix A.

We present the details of optimized *ESMM* implementation in Figure 4(b), where a thread block loads BLK input tokens each time based on the re-index vector, as well as the corresponding expert parameters. Since these BLK tokens are routed to the same expert, we only need to load one expert each time. We then accumulate the dot product results along the dimension of the input feature and write the result for each token back to its position in global memory, also based on the re-index vector. The details of optimized *ESS* is shown in Figure 4(c), where each thread block is employed to compute some channels of one expert, with BLK tokens one time. After accumulating all tokens within one expert, it writes the summation back to global memory. *ESTMM* is illustrated in Figure 4(d), where we present the input batches in a re-indexed manner. Specifically, the two input batches are the *ESMM* results of the same tensor,

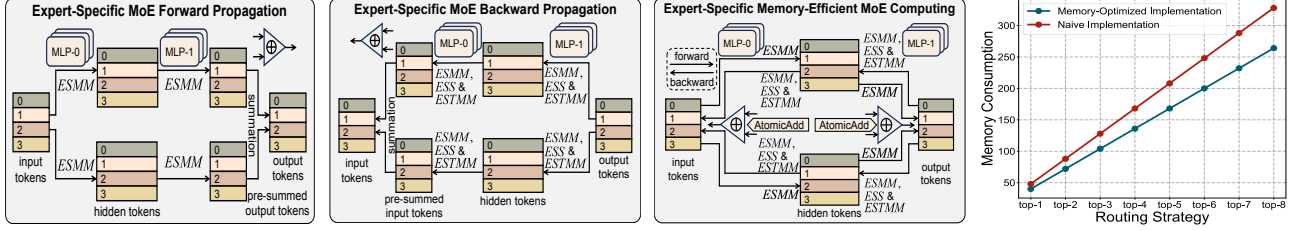


Figure 5: **Naive expert-specific MoE computing and the memory-efficient version.** We take top-2 routing and 4 tokens as an example. In the naive version, we have to compute from top-1 to top- k respectively, write each result back, and sum them up for the final output, while a memory-efficient version adopts AtomicAdd instead, saving much memory. We also present a comparison for the 2 schemes, assuming the memory for one input & output token as 1 and hidden token as 4.

sharing the same re-index vector. Each thread block loads BLK channels of both batches for tokens that are routed to the same expert. After accumulation, results are written back to the corresponding positions respectively. We also provide algorithm details of this part with PyTorch style pseudo-code in Appendix A.

Memory Optimization for Top- k Routing. We find that when extending the routing choice from top-1 to top- k , the memory consumption would increase significantly. To tackle this issue, we present a simplified pipeline in Figure 5, where only input, hidden, and output tokens in one MoE layer are provided. For naive forward propagation in Figure 5(a) and backward in Figure 5(b), we have to compute the result of all the k routing choices and sum them up to obtain the final output. Specifically, in forward propagation, we have to sum up the outputs of *ESMM* for the second MLP layer to get the output tokens, while in backward propagation we have to sum up the outputs of *ESMM* for the first MLP layer to get the gradients for input tokens. This leads to extra memory allocation for pre-summed tensors, including pre-summed output tokens in forward and pre-summed input tokens in backward. To optimize memory consumption when scaling from top-1 routing to top- k , we only allocate memory for the hidden tokens, and sum up the result of each routing choice via *atomicAdd* in CUDA programming, as illustrated in Figure 5(c). This can result in obvious memory reduction, as we presented in Figure 5(d).

Fused Kernel in Backward Propagation. For a single multi-layer perception (MLP) $y = x \cdot W + b$, the gradients for x , W and b can be computed in parallel, as they are unrelated with each other. Therefore, we can integrate the implementation of *ESS*, *ESTMM*, and *ESMM* together into one kernel function named expert-specific fused kernel (*ESFK*) for better parallelism. However, directly integrating them is hard to implement, since the shape of thread blocks required for each operator and the implementation details for each operator vary a lot with each other. To this end, we set the shape of the thread block to be the same for each operator, and expand one dimension for *ESMM* and *ESS* so that the thread grids are all 3-dimensional. Taking a single FFN layer under top-1 routing as an example, where we present the shape of allocated thread block and thread grid

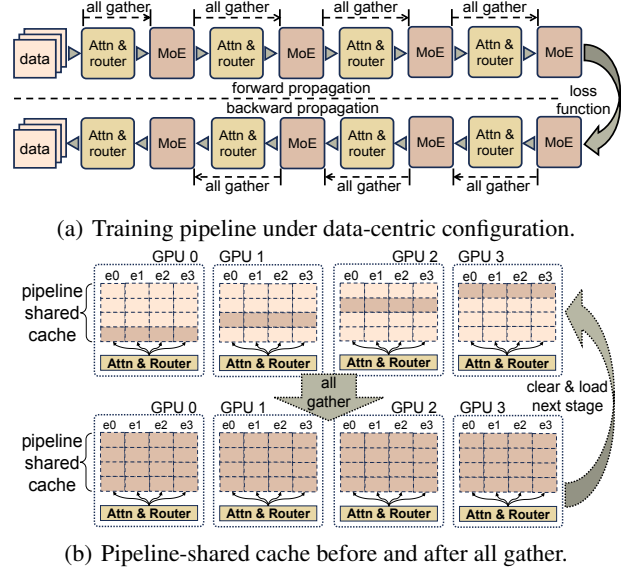


Figure 6: **Visualization of the training pipeline and shared cache under the data-centric setting.** Before all gather communication, each device loads the kept parameter chunk to its shared cache, after that each cache will be filled with the whole parameters of an MoE layer.

for both forward and backward propagation in Table 6 in Appendix B. By transposing the shape or expanding one dimension for the thread grid of an operator, we can align the 1st and 2nd dimensions while summing the 3rd dimension together for an integrated grid. In this way, the backward propagation for one FFN can be re-implemented with only 2 fused kernel function and 1 element-wise dot production.

4.3 Parallel Strategy for Different Workload Scale

Data Parallelism for Data-Centric Setting. Data-centric is a practical and efficient approach for both training and inference when the scale of the data batch is larger than the model parameters. HEXA-MoE distributes MoE parameters to different devices along the hidden size dimension of FFN, based on tensor parallelism. In a data-centric setting, each device gathers the whole MoE parameters from other devices and performs computing for each MoE layer locally, similar to data parallelism. Although MoE computing under data-centric configuration has been explored by Janus (Liu

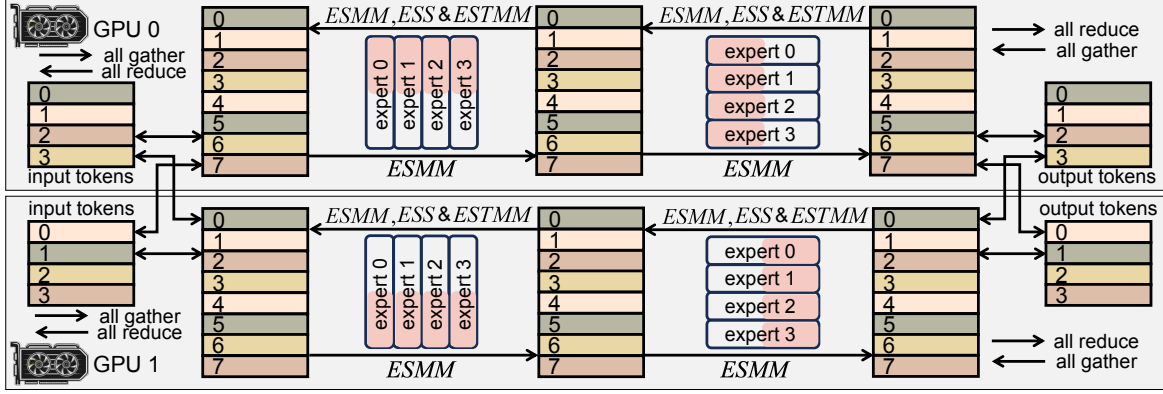


Figure 7: **Tensor parallelism for HEXA-MoE under model-centric setting.** Take 2 GPUs, 1 MoE layer, and 4 experts as an example, assuming the local batch contains 4 tokens. We refactor classical tensor parallelism with expert-specific operators.

et al., 2023), memory efficiency has not yet been fully studied. Janus pre-fetchs the required MoE parameters for each layer progressively in forward propagation and preserves all of them locally for backward propagation so that no communication is required when computing for gradients. However, the sheer size of MoE parameters can lead to a significant increase in memory usage, making it inefficient and impracticable for wider deployment.

To tackle this issue, we propose to allocate an additional region on the GPU memory of each device, which is adopted to dynamically cache the gathered MoE parameters for each pipeline stage, named as pipeline-shared cache. Since each device keeps a subset of the FFN hidden dimension for all experts in each layer, we need to employ all gather communication among devices before the computing of each MoE layer, preparing for the required parameters during both forward and backward propagation, as illustrated in Figure 6(a) and 6(b). To achieve better parallelism, all gather communication can be overlapped with other operations such as attention and router, as shown in Figure 6(a). In this way, each device would not have to preserve all the MoE parameters for backward propagation, while communication overhead can also be well masked, therefore both memory efficiency and computing efficiency can be achieved.

Tensor Parallelism for Model-Centric Setting. In the case that the scale of data is less than model parameters, model-centric configuration turns out to be more efficient than data-centric. To distribute MoE parameters on multiple devices, we modify the classical tensor parallelism with our proposed expert-specific operators, as shown in Figure 7. All gather communication is employed to synchronize local data batches before and after each MoE layer, and a pipeline-shared cache is not required in this setting. In Figure 1 we present a comparison between expert parallelism and tensor parallelism for the MoE layer, where HEXA-MoE takes small modification based on standard tensor parallelism (Narayanan et al., 2021). We distribute each MoE layer among different devices along the hidden size dimension for each expert, and during MoE computing, each

device computes the all gathered data batches with only the local MoE parameter chunk using *ESMM*, and the output tokens are all reduced with sum operation in forward propagation. During backward propagation, all gather and all reduce communications are interchanged, while *ESMM* are replaced by *ESMM*, *ESS*, and *ESTMM* to derive the gradients for input tokens, bias, and weights, respectively, which can also be replaced by the fused operator *ESFK*.

4.4 Heterogeneous-aware Expert Allocation

Workload Division for a different configuration. For data-centric configuration, since it can be essentially viewed as data parallelism, the workload mainly depends on batch size. For model-centric configuration, the workload of each device for the MoE layer mainly depends on the allocated sub-dimension of the hidden size with each expert, as we have replaced conventional expert parallelism with pure tensor parallelism with the aid of *expert-specific* operators.

Practical Expert Allocation on Heterogeneous Devices.

To adapt our HEXA-MoE to heterogeneous devices, we propose a specialized expert allocation approach that better utilizes the overall computing capacity by adjusting the workload on each device. Specifically, we have to first examine the computing capacity of each device by averaging its latency on the same proxy task of heavy computing, such as large-scale matrix multiplication or large-scale MLP computing. Denoting the results as $\{t_i\}_{i=0}^{N-1}$ for N devices that distribute the MoE model. For the data-centric setting, we assign different local batch size $\{B_i\}_{i=0}^{N-1}$ to different devices based on the observed latency, as shown in Equation 1:

$$B_i = \frac{1/t_i}{\sum_{j=0}^{N-1} 1/t_j} \cdot B_{\text{global}}, \quad (1)$$

where we denote B_{global} as the global batch size, i.e., $B_{\text{global}} = \sum_{j=0}^{N-1} B_j$. For the model-centric setting, we denote the sub-dimension of hidden size for one MoE layer on each device as $\{h_i\}_{i=0}^{N-1}$ with total hidden size H . The assigned sub-dimension h_i on device i can be derived as Equation 2.

$$h_i = \frac{1/t_i}{\sum_{j=0}^{N-1} 1/t_j} \cdot H. \quad (2)$$

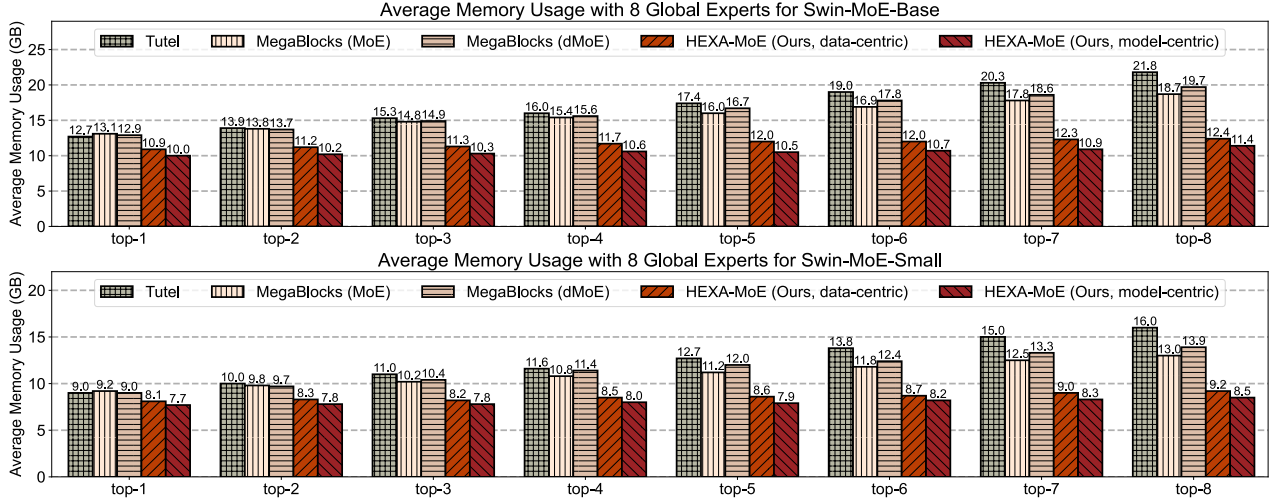


Figure 8: **Average memory usage for training Swin-Transformer-MoE models.** We take 8 global experts and examine all cases from top-1 to top-8 routings. Experiments are conducted on 2 homogeneous GPUs using automatic mixed precision in PyTorch. The batch size is set to 40 for all cases. We record the average GPU memory consumption (GB) on each device.

To ensure that both $\{B_i\}_{i=0}^{N-1}$ and $\{h_i\}_{i=0}^{N-1}$ are integers, we need to further round them up or down while making sure that the summation is exactly B_{global} or H .

5 EXPERIMENTS

5.1 Experimental Setup

We implement all the experiments using 2 machines, namely M_{homo} and M_{hete} . Specifically, M_{homo} is composed of 4 homogeneous GPUs, while M_{hete} contains 2 heterogeneous GPUs. Details for the machines and GPUs are provided in Table 2. We take the training process of Swin-Transformer-MoE as the benchmark for all the experiments, including memory analysis, latency analysis, heterogeneous computing analysis, and ablation studies. Apart from heterogeneous computing analysis, all the experiments are conducted on M_{homo} . We also adopt both the Small and Base scales for the Swin-MoE model, following Tutel (Hwang et al., 2023). Experiments are conducted with PyTorch, taking `nccl` as the communication backend. All the experiments are implemented in a distributed manner based on the distributed data-parallel interface in PyTorch, and batch size is the batch size on a single device rather than the global workload.

5.2 Experimental Results

Memory Analysis on Homogeneous Devices. We analyze the memory consumption for different MoE libraries on homogeneous devices. We adopt 8 global experts and examine all cases from top-1 routing to top-8. Results are visualized in Figure 8. HEXA-MoE can reduce 10%-48% memory usage compared to Tutel (Hwang et al., 2023) and MegaBlocks (Gale et al., 2023), and the memory usage for model-centric setting is slightly less than data-centric setting due to the employment of pipeline-shared cache. When scaling top-1 routing to top- k routing, the memory reduction becomes more significant, since we only enlarge the

Table 2: **Details of the machines and GPUs used for both homogeneous and heterogeneous experiments.**

	Notation	Number & Hardware Specs	Memory
CPU	M_{homo}	2× Intel Xeon Platinum 8352V 2.10GHz	1008 GB
	M_{hete}	2× Intel Xeon Gold 6130 2.10GHz	62.5 GB
GPU	D (in M_{homo})	4× NVIDIA GeForce RTX 4090	24 GB
	D_0 (in M_{hete})	1× NVIDIA TITAN RTX	24 GB
	D_1 (in M_{hete})	1× NVIDIA GeForce RTX 2080 Ti	11 GB

memory allocation for the hidden tokens, as illustrated in Figure 5. Meanwhile, the trend of memory consumption increase for our method is also much more gentle than Tutel and MegaBlocks when scaling from top-1 routing to top- k , owing to the introduction of memory-latency trade-off. Since HEXA-MoE performs MoE computing in an in-place manner and introduces no token padding, we can still save a certain amount of memory under top-1 routing.

Latency Analysis on Homogeneous Devices. We analyze the average latency for one training step, and present the results in Figure 9. To fully utilize the GPU memory, we set different batch sizes for different routing configurations and different model scales. HEXA-MoE achieves 0.5-4.3× speed up compared to Tutel (Hwang et al., 2023) and MegaBlocks (Gale et al., 2023). Since the scale of workload is larger than MoE parameters in our experiments, the average latency under a data-centric setting is less than model-centric in these cases, and the advantage of HEXA-MoE turns more obvious while enlarging batch size. To better visualize the latency comparison between data-centric and model-centric configurations, we present the latency for the Swin-MoE-Base model under different batch sizes in Figure 10. When the workload is relatively small, a model-centric setting is more efficient, while a data-centric setting becomes more efficient with a relatively large workload. Experiments are all conducted on the homogeneous machine

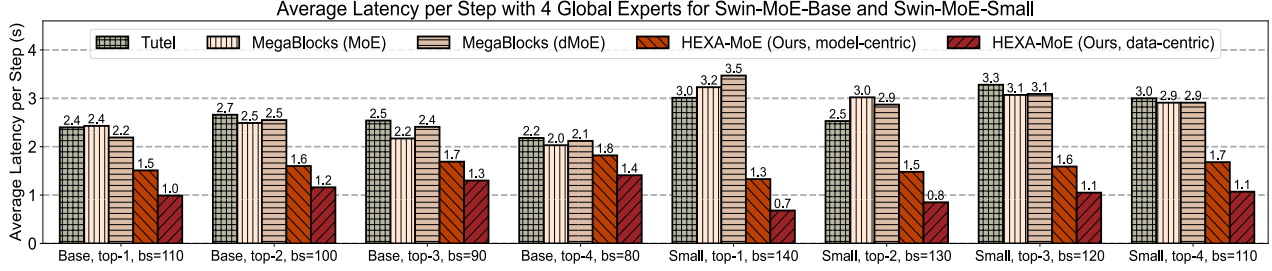


Figure 9: **Average latency for training Swin-Transformer-MoE models.** Experiments are conducted on 4 homogeneous GPUs with 4 global experts. We set different batch sizes for different models under different routing strategies to maximize the utilization of GPU memory. We record the average latency for one step (s) during training with 2k steps in total.

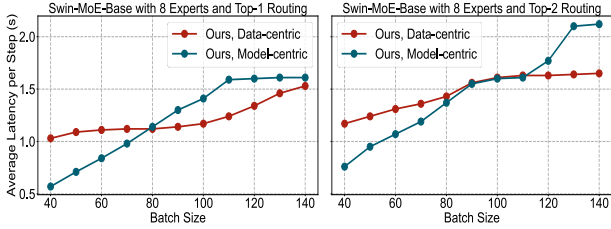


Figure 10: **Latency comparison with data-centric and model-centric configurations.** We record average latency per step with 2k steps in total. The data-centric setting presents a more gentle trend when scaling workload.

with automatic mixed precision in PyTorch.

Heterogeneous Experiments. We demonstrate the heterogeneous awareness of our HEXA-MoE via experiments on different devices under both data-centric and model-centric configurations, and visualize the average latency with different division strategies in Figure 11. Since the 2 GPUs in our heterogeneous machine have similar computing capacities, we also adjust the power limit for each device. We first examine the computing capacity for these experimental settings, and provide the results in Table 3. The details of the proxy task are provided in Appendix B.

In Figure 11(a), we adjust the batch size on each device under data-centric configuration. Essentially the optimal proportion is very close to the examined computing capacity proportion, and it has a certain deviation from uniform division when the power constraints of the two devices are not equal, while the optimal division is also uniform division when the power constraints are equal. Specifically, when setting the power constraint for D_0 to be 100W and D_1 to be 300W, employing our heterogeneous-aware allocation can make the average latency to be 13.2% lower than naive division, and when setting D_0 to be 300W and D_1 to be 100W, our approach can reduce the average latency by 25.3%.

In Figure 11(b), we adjust the allocated sub-dimension proportion of the hidden size for each MoE layer on each device. Adapting the sub-dimension proportion to be close to the computing capacity proportion of heterogeneous devices can also substantially minimize average latency, similar to the data-centric setting. Specifically, when setting the power

Table 3: **Examining computing capacity for heterogeneous devices.** P , T and R denote power constraint (W), average latency (s), and computing capacity proportion.

	Case 1			Case 2			Case 3		
	P	T	R	P	T	R	P	T	R
D_0	100	4.58	0.40	300	3.20	0.50	300	3.28	0.74
D_1	300	3.06	0.60	300	3.18	0.50	100	9.42	0.26

constraint of D_0 to be 100W and D_1 to be 300W, our approach can achieve a 6.3% reduction on average latency compared to uniform division, and when setting D_0 to be 300W and D_1 to be 100W, we can reduce it by 11.9%. Although the reduction is not as significant as a data-centric setting, we can still achieve a relative speed-up. These demonstrate that our HEXA-MoE can essentially maximize the utilization of heterogeneous computing resources.

5.3 Ablation Studies

We examine the effectiveness of each component for our HEXA-MoE via measuring the impact of expert-specific operators, pipeline-shared cache, fused kernel, data- & model-centric and memory-latency trade-off respectively on two indicators, *i.e.*, average latency and memory usage. We take the distributed training of the Swin-MoE-Base model on homogeneous devices as the benchmark for ablation study experiments. Since dispatch & combine operations are inevitable if we dispense with our expert-specific operators, we directly take the performance of Tutel in this case.

Memory Usage Breakdown. We take 8 experts, top-4 routing, and batch size 40 as an example to break down memory usage, and visualize the results in Figure 12(a). We can draw some insights from it:

- ★ The employment of pipeline-shared cache slightly increases memory consumption, while expert-specific fused kernel has no impact.
- ★ Pipeline-shared cache can effectively reduce memory consumption under a data-centric setting since the memory usage would surpass Tutel without it.
- ★ Our HEXA-MoE can reduce memory usage compared to baseline even without memory optimization, and optimizing it can further reduce memory consumption.

Latency Breakdown. We set 4 experts, top-4 routing, and batch size 80 to break down training latency, and visualize

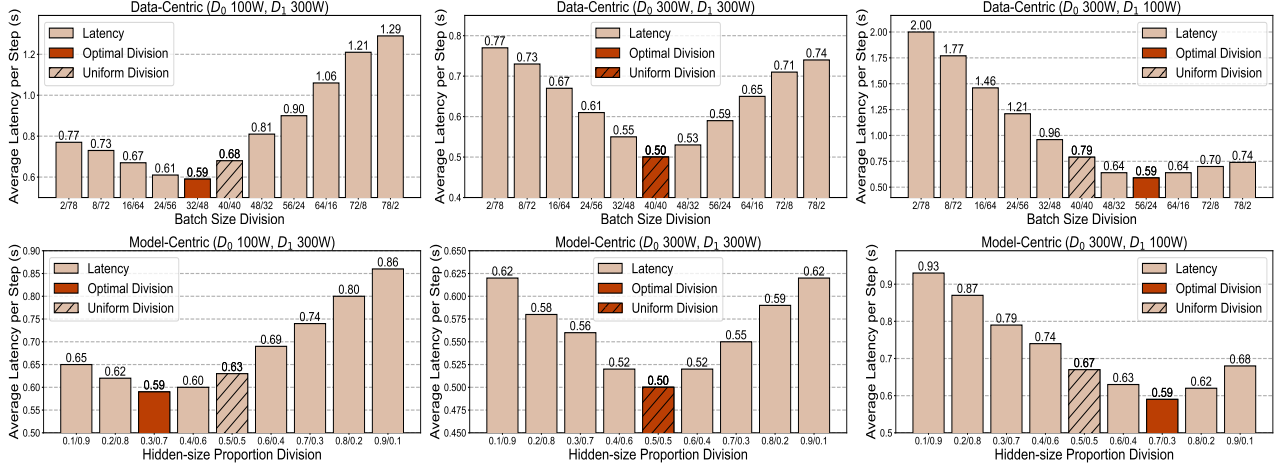


Figure 11: **Latency analysis on heterogeneous devices with both data-centric and model-centric configuration.** Experiments are all conducted with Swin-MoE-Small model using 4 global experts and top-2 routing. The average latency falls minimal when the division proportion is close to the computing capacity proportion in each case.

results in Figure 12(b). We can draw some insights as:

- ★ The employment of expert-specific fused kernel, data-centric setting, and communication-computation overlap can effectively reduce latency. Meanwhile, the combination of data-centric setting and communication-computation overlap can further empower our HEXA-MoE with notably reduced latency.
- ★ Expert-specific operators play a significant part in speeding up MoE computing since the latency for Tutel is much longer than our model-centric setting.
- ★ Although the employment of pipeline-shared cache and memory optimization would slightly increase latency, they can also lead to significant memory reduction, as demonstrated in memory usage breakdown.

6 CONCLUSION

In this paper, we analyze the limitations of current MoE libraries in detail and propose novel *expert-specific* operators as an alternative to GeMM so that MoE computing can be performed in an in-place manner with **zero** computation redundancy. We reformulate the forward and backward propagation of the MoE layer with these operators and replace conventional expert parallelism with tensor parallelism, *i.e.*, splitting the parameters of the MoE layer along the hidden size dimension to distribute them on different devices. We provide GPU implementations for these operators in a highly parallelized manner, which can both save memory consumption and reduce overall latency. For different workload scales, we implement the MoE model under both data- and model-centric configurations. To tackle the teaser of heavy memory consumption in previous data-centric works, we propose a pipeline-shared cache for better memory efficiency. Homogeneous experiments show that HEXA-MoE can save 10%-48% memory usage while achieving 0.5-4.3 \times speed up compared to state-of-the-art

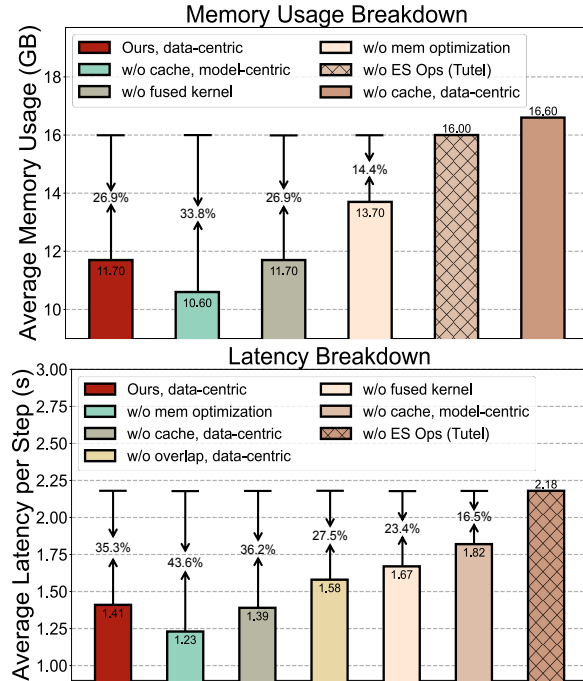


Figure 12: **Memory and latency breakdown.** We analyze the effectiveness of our proposed pipeline-shared cache, fused kernel, and memory-latency trade-off. We take Tutel as a baseline and visualize the differences with it.

MoE libraries. To adapt HEXA-MoE to heterogeneous devices, we propose to assign different batch sizes or sub-dimensions of hidden sizes for different devices based on the heterogeneous computing capacity. Experiments show that our adaption can substantially minimize average latency and better utilize the whole computing capacity. Meanwhile, our HEXA-MoE empowers MoE computing to be conducted in an in-place manner, *i.e.*, the routing choice would yield almost no impact on hardware workload, which can facilitate further research on MoE algorithms.

REFERENCES

- Bao, H., Wang, W., Dong, L., Liu, Q., Mohammed, O. K., Aggarwal, K., Som, S., Piao, S., and Wei, F. Vlmoe: Unified vision-language pre-training with mixture-of-modality-experts. *Advances in Neural Information Processing Systems*, 35:32897–32912, 2022.
- Choquette, J., Giroux, O., and Foley, D. Volta: Performance and programmability. *Ieee Micro*, 38(2):42–52, 2018.
- Deng, J., Dong, W., Socher, R., Li, L.-J., Li, K., and Fei-Fei, L. Imagenet: A large-scale hierarchical image database. In *2009 IEEE conference on computer vision and pattern recognition*, pp. 248–255. Ieee, 2009.
- Du, N., Huang, Y., Dai, A. M., Tong, S., Lepikhin, D., Xu, Y., Krikun, M., Zhou, Y., Yu, A. W., Firat, O., et al. Glam: Efficient scaling of language models with mixture-of-experts. In *International Conference on Machine Learning*, pp. 5547–5569. PMLR, 2022.
- Fan, Z., Sarkar, R., Jiang, Z., Chen, T., Zou, K., Cheng, Y., Hao, C., Wang, Z., et al. M³vit: Mixture-of-experts vision transformer for efficient multi-task learning with model-accelerator co-design. *Advances in Neural Information Processing Systems*, 35:28441–28457, 2022.
- Fedus, W., Zoph, B., and Shazeer, N. Switch transformers: Scaling to trillion parameter models with simple and efficient sparsity. *Journal of Machine Learning Research*, 23(120):1–39, 2022.
- Gale, T., Narayanan, D., Young, C., and Zaharia, M. Megablocks: Efficient sparse training with mixture-of-experts. *Proceedings of Machine Learning and Systems*, 5:288–304, 2023.
- He, J., Qiu, J., Zeng, A., Yang, Z., Zhai, J., and Tang, J. Fastmoe: A fast mixture-of-expert training system. *arXiv preprint arXiv:2103.13262*, 2021.
- He, J., Zhai, J., Antunes, T., Wang, H., Luo, F., Shi, S., and Li, Q. Fastermoe: modeling and optimizing training of large-scale dynamic pre-trained models. In *Proceedings of the 27th ACM SIGPLAN Symposium on Principles and Practice of Parallel Programming*, pp. 120–134, 2022a.
- He, K., Chen, X., Xie, S., Li, Y., Dollár, P., and Girshick, R. Masked autoencoders are scalable vision learners. In *Proceedings of the IEEE/CVF conference on computer vision and pattern recognition*, pp. 16000–16009, 2022b.
- Hwang, C., Cui, W., Xiong, Y., Yang, Z., Liu, Z., Hu, H., Wang, Z., Salas, R., Jose, J., Ram, P., et al. Tutel: Adaptive mixture-of-experts at scale. *Proceedings of Machine Learning and Systems*, 5:269–287, 2023.
- Jiang, A. Q., Sablayrolles, A., Roux, A., Mensch, A., Savary, B., Bamford, C., Chaplot, D. S., Casas, D. d. l., Hanna, E. B., Bressand, F., et al. Mixtral of experts. *arXiv preprint arXiv:2401.04088*, 2024.
- Kaplan, J., McCandlish, S., Henighan, T., Brown, T. B., Chess, B., Child, R., Gray, S., Radford, A., Wu, J., and Amodei, D. Scaling laws for neural language models. *arXiv preprint arXiv:2001.08361*, 2020.
- Lepikhin, D., Lee, H., Xu, Y., Chen, D., Firat, O., Huang, Y., Krikun, M., Shazeer, N., and Chen, Z. Gshard: Scaling giant models with conditional computation and automatic sharding. In *International Conference on Learning Representations*, 2020.
- Li, J., Li, D., Xiong, C., and Hoi, S. Blip: Bootstrapping language-image pre-training for unified vision-language understanding and generation. In *International conference on machine learning*, pp. 12888–12900. PMLR, 2022.
- Li, J., Jiang, Y., Zhu, Y., Wang, C., and Xu, H. Accelerating distributed {MoE} training and inference with lina. In *2023 USENIX Annual Technical Conference (USENIX ATC 23)*, pp. 945–959, 2023.
- Liu, H., Li, C., Wu, Q., and Lee, Y. J. Visual instruction tuning. *Advances in neural information processing systems*, 36, 2024.
- Liu, J., Wang, J. H., and Jiang, Y. Janus: A unified distributed training framework for sparse mixture-of-experts models. In *Proceedings of the ACM SIGCOMM 2023 Conference*, pp. 486–498, 2023.
- Liu, Z., Lin, Y., Cao, Y., Hu, H., Wei, Y., Zhang, Z., Lin, S., and Guo, B. Swin transformer: Hierarchical vision transformer using shifted windows. In *Proceedings of the IEEE/CVF international conference on computer vision*, pp. 10012–10022, 2021.
- Narayanan, D., Shoeybi, M., Casper, J., LeGresley, P., Patwary, M., Korthikanti, V., Vainbrand, D., Kashinkunti, P., Bernauer, J., Catanzaro, B., et al. Efficient large-scale language model training on gpu clusters using megatron-lm. In *Proceedings of the International Conference for High Performance Computing, Networking, Storage and Analysis*, pp. 1–15, 2021.
- Raffel, C., Shazeer, N., Roberts, A., Lee, K., Narang, S., Matena, M., Zhou, Y., Li, W., and Liu, P. J. Exploring the limits of transfer learning with a unified text-to-text transformer. *Journal of machine learning research*, 21(140):1–67, 2020.

Riquelme, C., Puigcerver, J., Mustafa, B., Neumann, M., Jenatton, R., Susano Pinto, A., Keyzers, D., and Houlsby, N. Scaling vision with sparse mixture of experts. *Advances in Neural Information Processing Systems*, 34: 8583–8595, 2021.

Shi, S., Pan, X., Chu, X., and Li, B. Pipemoe: Accelerating mixture-of-experts through adaptive pipelining. In *IEEE INFOCOM 2023-IEEE Conference on Computer Communications*, pp. 1–10. IEEE, 2023.

Shi, S., Pan, X., Wang, Q., Liu, C., Ren, X., Hu, Z., Yang, Y., Li, B., and Chu, X. Schemoe: An extensible mixture-of-experts distributed training system with tasks scheduling. In *Proceedings of the Nineteenth European Conference on Computer Systems*, pp. 236–249, 2024.

Vaswani, A. Attention is all you need. *Advances in Neural Information Processing Systems*, 2017.

Zhai, M., He, J., Ma, Z., Zong, Z., Zhang, R., and Zhai, J. {SmartMoE}: Efficiently training {Sparsely-Activated} models through combining offline and online parallelization. In *2023 USENIX Annual Technical Conference (USENIX ATC 23)*, pp. 961–975, 2023.

Zhang, Z., Xia, Y., Wang, H., Yang, D., Hu, C., Zhou, X., and Cheng, D. Mpmoe: Memory efficient moe for pre-trained models with adaptive pipeline parallelism. *IEEE Transactions on Parallel and Distributed Systems*, 2024.

A ALGORITHM DETAILS

We present the algorithm details for re-index vector construction as well as the expert-specific operators, and taking top-1 routing as an example for illustration, shown in Algorithm 1, 3, 2 and 4. In Algorithm 1, we re-arrange the routing choice vector \mathcal{R} into re-indexed token vector v , along with the token index starting vector idx , which satisfies $idx[0] = 0$ and $idx[E] = N'$. We provide the length and range for the vectors in Table 4.

Table 4: Explanation for the auxiliary vectors.

vector	length	range
\mathcal{R}	N	$0 \leq \mathcal{R}[i] < E$ for $0 \leq i < N$
v	N'	$0 \leq v[i] < N$ for $0 \leq i < N'$
idx	$1 + E$	$0 \leq idx[i] < N'$ for $0 \leq i < 1 + E$

In Algorithm 3, 2 and 4, we assume that the feature dimension for each tensor is all divisible by BLK. Notice that when accessing the re-index vector v , we may get value -1, since the workload for each expert is dynamic. In this case, we would skip this index, and remain zero for the temporary loading variable.

We also provide the formulation for top- k routing with our expert-specific operators, and take a comparison with top-1 routing. We denote the routing choice for top- k as $\{\mathcal{R}_i(\mathbf{x})\}_{i=0}^{k-1}$, and other symbols keep consistent with Figure 3. We present the comparison on formulations for MoE forward and backward propagation in Table 5.

Algorithm 1 Constructing re-index vector

Input: Routing choice \mathcal{R} with shape $(N,)$.
Initialize: Tensor ctr with shape $(E,)$ initialized with 0.
Parallel for $i = 0$ **to** $N - 1$ **do**
 $\text{atomicAdd}(ctr[\mathcal{R}[i]], 1)$
end for
Parallel for $i = 0$ **to** $E - 1$ **do**
 $ctr[i] = \text{BLK} \cdot \lfloor ctr[i] / \text{BLK} \rfloor$
end for
 $N' = \sum_{i=0}^{E-1} ctr[i]$
Initialize: Tensor v with shape $(N',)$ initialized with -1, and tensor idx with shape $(1 + E,)$ initialized with 0.
Parallel for $i = 0$ **to** $E - 1$ **do**
 $ctr[i] = \text{BLK} \cdot \lfloor ctr[i] / \text{BLK} \rfloor$
end for
for $i = 1$ **to** E **do**
 $idx[i] = idx[i - 1] + ctr[i - 1]$
end for
Copy: $idx_ = idx$
Parallel for $i = 0$ **to** $N - 1$ **do**
 $pos = \text{atomicAdd}(idx[\mathcal{R}[i]], 1)$
 $v[pos] = i$
end for
Output: Tensor v and $idx_$

B EXPERIMENTAL DETAILS

We provide the details of our CUDA program via enumerating the shape of the thread block and thread grid for expert-specific operators in a single MoE layer in Table 6.

We also provide the Python code for the proxy task we used to examine the computing capacity of the heterogeneous devices. We adopt a for loop composed of large matrix multiplications with the same scale as the test program, as provided below:

```
import torch
import time

device = 'cuda'
size = 2048
times = 1024

start_time = time.time()
for j in range(times):
    mat1 = torch.randn(size, size, device=device)
    mat2 = torch.randn(size, size, device=device)
    y = torch.matmul(mat1, mat2)
end_time = time.time()

print(end_time - start_time)
```

Table 5: Comparison between top-1 and top- k routing for the formulation of MoE forward and backward with our expert-specific operators.

Stage	Notation	Layer	Expert-Specific Formulation (top-1 routing)	Expert-Specific Formulation (top- k routing)
Forward	①	1st MLP	$\mathbf{y}_1 = \text{ESMM}(\mathbf{x}, \mathbf{W}_1, \mathbf{b}_1, \mathcal{R}(\mathbf{x}))$	$\{\mathbf{y}_1^i\}_{i=0}^{k-1} : \mathbf{y}_1^i = \text{ESMM}(\mathbf{x}, \mathbf{W}_1, \mathbf{b}_1, \mathcal{R}_i(\mathbf{x}))$
	②	Activation	$\mathbf{y}_2 = \mathcal{F}(\mathbf{y}_1)$	$\{\mathbf{y}_2^i\}_{i=0}^{k-1} : \mathbf{y}_2^i = \mathcal{F}(\mathbf{y}_1^i)$
	③	2nd MLP	$\mathbf{y} = \text{ESMM}(\mathbf{y}_2, \mathbf{W}_2, \mathbf{b}_2, \mathcal{R}(\mathbf{x}))$	$\mathbf{y} = \sum_{i=0}^{k-1} \text{ESMM}(\mathbf{y}_2^i, \mathbf{W}_2, \mathbf{b}_2, \mathcal{R}_i(\mathbf{x}))$
Backward	④	2nd MLP	$\frac{\partial \ell}{\partial \mathbf{b}_2} = \text{ESS}(\frac{\partial \ell}{\partial \mathbf{y}}, \mathcal{R}(\mathbf{x}))$	$\frac{\partial \ell}{\partial \mathbf{b}_2} = \sum_{i=0}^{k-1} \text{ESS}(\frac{\partial \ell}{\partial \mathbf{y}}, \mathcal{R}_i(\mathbf{x}))$
	⑤		$\frac{\partial \ell}{\partial \mathbf{W}_1} = \text{ESTMM}(\mathbf{x}, \frac{\partial \ell}{\partial \mathbf{y}_1}, \mathcal{R}(\mathbf{x}))$	$\frac{\partial \ell}{\partial \mathbf{W}_1} = \sum_{i=0}^{k-1} \text{ESTMM}(\mathbf{x}, \frac{\partial \ell}{\partial \mathbf{y}_1^i}, \mathcal{R}_i(\mathbf{x}))$
	⑥		$\frac{\partial \ell}{\partial \mathbf{y}_2} = \text{ESMM}(\frac{\partial \ell}{\partial \mathbf{y}}, \mathbf{W}_2^T, \text{null}, \mathcal{R}(\mathbf{x}))$	$\left\{ \frac{\partial \ell}{\partial \mathbf{y}_2^i} \right\}_{i=0}^{k-1} : \frac{\partial \ell}{\partial \mathbf{y}_2^i} = \text{ESMM}(\frac{\partial \ell}{\partial \mathbf{y}}, \mathbf{W}_2^T, \text{null}, \mathcal{R}_i(\mathbf{x}))$
	⑦	Activation	$\frac{\partial \ell}{\partial \mathbf{y}_1} = \frac{\partial \ell}{\partial \mathbf{y}_2} \odot \mathcal{F}'(\mathbf{y}_1)$	$\left\{ \frac{\partial \ell}{\partial \mathbf{y}_1^i} \right\}_{i=0}^{k-1} : \frac{\partial \ell}{\partial \mathbf{y}_1^i} = \frac{\partial \ell}{\partial \mathbf{y}_2^i} \odot \mathcal{F}'(\mathbf{y}_1^i)$
	⑧	1st MLP	$\frac{\partial \ell}{\partial \mathbf{b}_1} = \text{ESS}(\frac{\partial \ell}{\partial \mathbf{y}_1}, \mathcal{R}(\mathbf{x}))$	$\frac{\partial \ell}{\partial \mathbf{b}_1} = \sum_{i=0}^{k-1} \text{ESS}(\frac{\partial \ell}{\partial \mathbf{y}_1^i}, \mathcal{R}_i(\mathbf{x}))$
	⑨		$\frac{\partial \ell}{\partial \mathbf{W}_1} = \text{ESTMM}(\mathbf{x}, \frac{\partial \ell}{\partial \mathbf{y}_1}, \mathcal{R}(\mathbf{x}))$	$\frac{\partial \ell}{\partial \mathbf{W}_1} = \sum_{i=0}^{k-1} \text{ESTMM}(\mathbf{x}, \frac{\partial \ell}{\partial \mathbf{y}_1^i}, \mathcal{R}_i(\mathbf{x}))$
	⑩		$\frac{\partial \ell}{\partial \mathbf{x}} = \text{ESMM}(\frac{\partial \ell}{\partial \mathbf{y}_1}, \mathbf{W}_1^T, \text{null}, \mathcal{R}(\mathbf{x}))$	$\frac{\partial \ell}{\partial \mathbf{x}} = \sum_{i=0}^{k-1} \text{ESMM}(\frac{\partial \ell}{\partial \mathbf{y}_1^i}, \mathbf{W}_1^T, \text{null}, \mathcal{R}_i(\mathbf{x}))$

Algorithm 2 Expert-specific summation

Input: Routing choice \mathcal{R} with shape $(N,)$, vector v with length N' , vector idx with length $1 + E$ and input tokens x with shape (N, D)

Initialize: Output tokens y with shape (E, D) initialized with 0.

Parallel for $i = 0$ **to** $E - 1$ **do**

Parallel for j **in range** $(0, D, \text{BLK})$ **do**

$exp = \mathcal{R}[v[idx[i]]]$

Initialize zero tensor c with shape $(1, \text{BLK})$

Initialize zero tensor x_{sub} with shape (BLK, BLK)

for k **in range** $(idx[i], idx[i + 1], \text{BLK})$ **do**

Parallel for $t = 0$ **to** BLK **do**

 load $x_{sub}[t] = x[v[k + t], j : j + \text{BLK}]$

end for

$c = c + \sum_{t=0}^{\text{BLK}-1} x_{sub}[t]$

end for

Write back: $y[exp, j : j + \text{BLK}] = c$

end for

end for

Output: Tensor y

Swin-MoE-Base with 4 experts and top-1 routing as the backbone network, training it on the homogeneous machine with the same batch size using Imagenet-1k dataset (Deng et al., 2009). Since our HEXA-MoE can accelerate training process, its validation accuracy is much higher than baseline.

C EXPERIMENTAL RESULTS

We provide the exact values for both memory usage analysis and average latency analysis in Table 7 and 8, respectively. Specifically, for latency analysis, we provide the average value for each case with 0.5k, 1k, 1.5k and 2k total steps.

We also visualize the validation accuracy of our method and Tutel under the same training time in Figure 13. We take

Table 6: **Shape of the thread block and thread grid for expert-specific operators in one MoE layer.** We take top-1 routing as an example, where N' denotes the length of the re-index vector, which is slightly larger than N and is divisible by BLK. Thread blocks are all defined with the same shape to facilitate the fused kernel.

	Operator	Input		Output		Thread Block	Thread Grid
forward	ESMM	\mathbf{x}	(N, D_1)	\mathbf{y}	(N, D_2)	(WARP, TIMES)	$(\lceil N'/\text{BLK} \rceil, \lceil D_2/(\text{TIMES} \cdot \text{BLK}) \rceil)$
		\mathbf{w}	(E, D_1, D_2)				
		\mathbf{b}	(E, D_2)				
backward	ESMM	\mathbf{x}	(N, D_2)	\mathbf{y}	(N, D_1)	(WARP, TIMES)	$(\lceil N'/\text{BLK} \rceil, \lceil D_1/(\text{TIMES} \cdot \text{BLK}) \rceil)$
		\mathbf{w}	(E, D_2, D_1)				
	ESS	\mathbf{x}	(N, D_2)	\mathbf{y}	(E, D_2)	(WARP, TIMES)	$(E, \lceil D_2/(\text{TIMES} \cdot \text{BLK}) \rceil)$
	ESTMM	\mathbf{x}_1	(N, D_1)	\mathbf{w}	(E, D_1, D_2)	(WARP, TIMES)	$(\lceil D_2/\text{BLK} \rceil, \lceil D_1/(\text{TIMES} \cdot \text{BLK}) \rceil, E)$
		\mathbf{x}_2	(N, D_2)				
	ESFK	\mathbf{x}_1	(N, D_1)	\mathbf{y}_1	(N, D_1)	(WARP, TIMES)	$(E, \lceil D_1/(\text{TIMES} \cdot \text{BLK}) \rceil, \lceil N'/\text{BLK} \rceil + \lceil D_2/\text{BLK} \rceil + \lceil D_2/(\text{TIMES} \cdot \text{BLK}) \rceil)$
		\mathbf{x}_2	(N, D_2)	\mathbf{y}_2	(E, D_2)		
		\mathbf{w}_1	(E, D_2, D_1)	\mathbf{w}_2	(E, D_1, D_2)		

Algorithm 3 Expert-specific matrix multiplication

Input: Routing choice \mathcal{R} with shape $(N,)$, vector v with length N' , input tokens x with shape (N, D_1) , weights w with shape (E, D_1, D_2) and bias b with shape (E, D_2)
Initialize: Output tokens y with shape (N, D_2) initialized with 0.

```

Parallel for  $i$  in range  $(0, N', \text{BLK})$  do
    Parallel for  $j$  in range  $(0, D_2, \text{BLK})$  do
         $\text{exp} = \mathcal{R}[v[i]]$ 
        Initialize zero tensor  $c$  with shape  $(\text{BLK}, \text{BLK})$ 
        load  $b_{\text{sub}} = b[\text{exp}, j : j + \text{BLK}]$ 
         $c = b_{\text{sub}}.\text{repeat}(\text{BLK}, 1)$ 
        for  $k$  in range  $(0, D_1, \text{BLK})$  do
            Initialize zero tensor  $x_{\text{sub}}$  with shape  $(\text{BLK}, \text{BLK})$ 
            Parallel for  $t = 0$  to  $\text{BLK}$  do
                load  $x_{\text{sub}}[t] = x[v[i + t], k : k + \text{BLK}]$ 
            end for
            load  $w_{\text{sub}} = w[\text{exp}, k : k + \text{BLK}, j : j + \text{BLK}]$ 
             $c = c + x_{\text{sub}} \cdot w_{\text{sub}}$ 
        end for
        Parallel for  $t = 0$  to  $\text{BLK}$  do
            Write back:  $y[v[i + t], j : j + \text{BLK}] = c[t]$ 
        end for
    end for
end for
Output: Tensor  $y$ 
    
```

Algorithm 4 Expert-specific transposed matrix multiplication

Input: Routing choice \mathcal{R} with shape $(N,)$, vector v with length N' , vector idx with length $1 + E$, the first token batch x_1 with shape (N, D_1) and the second token batch x_2 with shape (N, D_2)

Initialize: Output y with shape (E, D_1, D_2) initialized with 0.

```

Parallel for  $i = 0$  to  $E - 1$  do
    Parallel for  $m$  in range  $(0, D_1, \text{BLK})$  do
        Parallel for  $n$  in range  $(0, D_2, \text{BLK})$  do
             $\text{exp} = \mathcal{R}[v[\text{idx}[i]]]$ 
            Initialize zero tensor  $c$  with shape  $(\text{BLK}, \text{BLK})$ 
            Initialize zero tensor  $x_{\text{sub}}^1$  with shape  $(\text{BLK}, \text{BLK})$ 
            Initialize zero tensor  $x_{\text{sub}}^2$  with shape  $(\text{BLK}, \text{BLK})$ 
            for  $k$  in range  $(\text{idx}[i], \text{idx}[i + 1], \text{BLK})$  do
                Parallel for  $t = 0$  to  $\text{BLK}$  do
                    load  $x_{\text{sub}}^1[t] = x_1[v[k + t], m : m + \text{BLK}]$ 
                    load  $x_{\text{sub}}^2[t] = x_2[v[k + t], n : n + \text{BLK}]$ 
                end for
                 $c = c + x_{\text{sub}}^1.\text{transpose}() \cdot x_{\text{sub}}^2$ 
            end for
            Write back in parallel:
                 $y[\text{exp}, m : m + \text{BLK}, n : n + \text{BLK}] = c$ 
        end for
    end for
end for
Output: Tensor  $y$ 
    
```

Table 7: **Memory analysis with Tutel, MegaBlocks and HEXA-MoE on Swin-Transformer-MoE benchmark (Base and Small).** Experiments are conducted on 2 homogeneous GPUs with automatic mixed precision in PyTorch and batch size 40 for all the experiments. We set the number of global experts to 8, and record the average GPU memory consumption (GB) on each device.

	Method	top-1	top-2	top-3	top-4	top-5	top-6	top-7	top-8
Base	Tutel	12.7	13.9	15.3	16.0	17.4	19.0	20.3	21.8
	MegaBlocks (MoE)	13.1	13.8	14.8	15.4	16.0	16.9	17.8	18.7
	MegaBlocks (dMoE)	12.9	13.7	14.9	15.6	16.7	17.8	18.6	19.7
	Ours (data-centric)	10.9	11.2	11.3	11.7	12.0	12.0	12.3	12.4
	Ours (model-centric)	10.0	10.2	10.3	10.6	10.5	10.7	10.9	11.4
Small	Tutel	9.0	10.0	11.0	11.6	12.7	13.8	15.0	16.0
	MegaBlocks (MoE)	9.2	9.8	10.2	10.8	11.2	11.8	12.5	13.0
	MegaBlocks (dMoE)	9.0	9.7	10.4	11.4	12.0	12.4	13.3	13.9
	Ours (data-centric)	8.1	8.3	8.2	8.5	8.6	8.7	9.0	9.2
	Ours (model-centric)	7.7	7.8	7.8	8.0	7.9	8.2	8.3	8.5

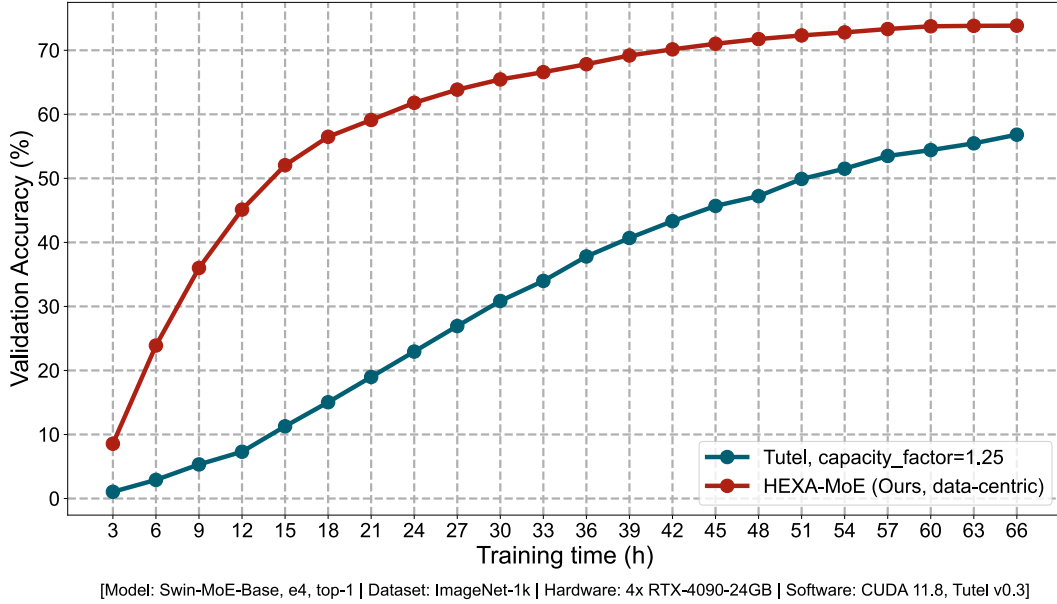


Figure 13: **Comparison on validation accuracy for Tutel and HEXA-MoE with the same training time.** HEXA-MoE has a significant advantage over Tutel due to the highly improved efficiency on computation.

Table 8: **Latency analysis for Tutel, MegaBlocks and HEXA-MoE on Swin-Transformer-MoE benchmark with base and small scale.** Experiments are conducted on 4 homogeneous GPUs with 4 experts. We set different batch size (bs) for different models under different routing strategy to maximize the utilization of GPU memory. We record the average latency of one step (s) during training.

		Method	0.5k	1k	1.5k	2k		0.5k	1k	1.5k	2k
Base	top-1, bs=110	Tutel	2.96	2.90	2.47	2.40	top-2, bs=100	2.14	2.59	2.73	2.66
		MegaBlocks (MoE)	2.10	2.66	2.57	2.43		2.40	2.58	2.51	2.49
		MegaBlocks (dMoE)	2.06	2.02	2.13	2.19		2.47	2.72	2.63	2.55
		Ours (model-centric)	1.52	1.51	1.51	1.51		1.61	1.60	1.60	1.60
		Ours (data-centric)	1.01	0.99	0.99	0.99		1.17	1.16	1.16	1.16
	top-3, bs=90	Tutel	2.23	2.43	2.48	2.54	top-4, bs=80	2.27	2.34	2.20	2.18
		MegaBlocks (MoE)	2.09	2.31	2.35	2.17		2.11	2.18	2.05	2.03
		MegaBlocks (dMoE)	2.55	2.53	2.44	2.41		2.00	2.19	2.23	2.12
		Ours (model-centric)	1.70	1.69	1.69	1.69		1.83	1.82	1.82	1.82
		Ours (data-centric)	1.32	1.31	1.31	1.30		1.42	1.41	1.41	1.41
Small	top-1, bs=140	Tutel	3.59	3.63	3.62	3.01	top-2, bs=130	2.83	2.96	2.72	2.53
		MegaBlocks (MoE)	3.41	3.64	3.72	3.23		3.04	3.26	3.11	3.02
		MegaBlocks (dMoE)	3.51	3.58	3.76	3.47		2.25	3.10	3.01	2.87
		Ours (model-centric)	1.34	1.34	1.33	1.33		1.49	1.49	1.48	1.48
		Ours (data-centric)	0.69	0.68	0.68	0.68		0.87	0.86	0.86	0.85
	top-3, bs=120	Tutel	2.23	2.92	3.17	3.28	top-4, bs=110	3.09	2.86	3.03	3.00
		MegaBlocks (MoE)	2.63	2.79	2.92	3.07		3.04	3.09	3.01	2.91
		MegaBlocks (dMoE)	3.08	3.24	3.38	3.09		3.03	3.19	3.18	2.91
		Ours (model-centric)	1.61	1.60	1.59	1.59		1.67	1.67	1.68	1.68
		Ours (data-centric)	1.07	1.05	1.05	1.05		1.09	1.08	1.07	1.07